J|A|C|S ARTICLES

Published on Web 07/13/2009

Cubane-Type Co_4S_4 Clusters: Synthesis, Redox Series, and Magnetic Ground States

Liang Deng,[†] Eckhard Bill,[‡] Karl Wieghardt,[‡] and R. H. Holm*,[†]

Department of Chemistry and Chemical Biology, Harvard University, Cambridge, Massachusetts 02138, and Max-Planck-Institut für Bioanorganische Chemie, Mülheim an der Ruhr, Germany

Received May 15, 2009; E-mail: holm@chemistry.harvard.edu

Abstract: The recent demonstration that the carbene cluster $[Fe_4S_4(Pr^i_2NHCMe_2)_4]$ (**9**) is an accurate structural and electronic analogue of the fully reduced cluster of the iron protein of *Azotobacter vinelandii* nitrogenase, including a common $S = 4$ ground state, raises the issue of the existence and magnetism of other $[M_4S_4L_4]^z$ clusters, none of which are known with transition metals other than iron. The system $CoCl_2$/Pr^i_3P/$(Me_3Si)_2S$/THF assembles $[Co_4S_4(PPr^i_3)_4]$ (**3**), which is converted to $[Co_4S_4(Pr^i_2NHCMe_2)_4]$ (**5**) upon reaction with carbene. The clusters support the redox series $[\mathbf{3}]^{1-/0/1+}$ and $[\mathbf{5}]^{0/1+/2+}$; monocations (**4**, **6**) have been isolated by chemical oxidation. Redox potentials and substitution reactions indicate that the carbene is the more effective electron donor to tetrahedral Fe^{II} and Co^{II} sites. Clusters **3**−**6** have the same overall cubane-type geometry as **9**. Neutral clusters **3** and **5** have an $S = 3$ ground state. As with the $S = 4$ state of **9** with local spins $S_{Fe} = 2$, the septet spin state can be described in terms of the coupling of three parallel and one antiparallel spins $S_{Co} = 3/2$. The octanuclear clusters $[Co_8S_8(PPr^i_3)_6]^{0,1+}$ were isolated as minor byproducts of the formation and chemical oxidation of **3**. The clusters exhibit a rhomb-bridged noncubane (RBNC) structure, whereas clusters with the Fe_8S_8 core possess edge-bridged double-cubane (EBDC) stereochemistry. There are two structural solutions for the M_8S_8 core in the form of topological isomers whose stability may depend on valence electron count. A conceptual model for the RBNC ↔ EBDC interconversion is presented. ($Pr^i_2NHCMe_2 = C_{11}H_{20}N_2$ = 1,3-diisopropyl-4,5-dimethylimidazol-2-ylidene).

Introduction

The cubane-type core unit $Fe_4(\mu_3\text{-}S)_4$ is prominently represented within the vast array of structures of iron−sulfur clusters with weak field[1−3] and strong field[4] terminal ligands. Our interest in weak field clusters derives from their well-known role as accurate structural and electronic analogues of protein-bound clusters $[Fe_4S_4(S_{Cys})_3L]$ in which ligand L is cysteinate, another amino acid side chain, or hydroxide/water.[2] In such clusters the core oxidation states $[Fe_4S_4]^{3+,2+,1+}$ are common, and all have been isolated in synthetic clusters.[2] The demonstration of the all-ferrous oxidation state $[Fe_4S_4]^0$ in the iron protein of *Azotobacter vinelandii* (*Av*) nitrogenase[5−8] and more recently in a dehydratase activator protein from *Acidaminococcus fermentans*,[9] upon reduction of the proteins with Ti(III) citrate, provided an imperative for the synthesis and full characterization of heretofore unknown synthetic analogues of this state. The first all-ferrous clusters produced were the phosphine species $[Fe_4S_4(PR_3)_4]$ (R = Pr^i, Bu^t, C_6H_{11}), but all attempts to isolate these compounds in substance resulted in core aggregation accompanying phosphine dissociation to afford the dicubanes $[Fe_8S_8(PR_3)_6]$ and tetracubanes $[Fe_{16}S_{16}(PR_3)_8]$.[10,11] More recently, fully reduced clusters have been isolated in the form of $[Fe_4S_4(CN)_4]^{4-}$ [12] and $[Fe_4S_4(Pr^i_2NHCMe_2)_4]$ with the *N*-heterocyclic carbene ligand 1,3-diisopropyl-4,5-dimethylimidazol-2-ylidene.[13] The more stable carbene cluster has been shown to be a meaningful representation of the all-ferrous cluster in proteins.[13,14] In particular, a detailed analysis of its Mössbauer and EPR spectra has established an $S_t = 4$ ground state,[15] which among all biological clusters has been found only in those of the *Av* iron protein[7] and the activator protein.[9]

The foregoing results support the proposition that the exchange coupling leading to the observed ground state is intrinsic to the $[Fe_4S_4]^0$ core and is not significantly influenced by the terminal ligands. An associated issue is the ground spin states in other fully reduced cubane-type $[M_4S_4]^0$ clusters with

[†] Harvard University.
[‡] Max-Planck-Institut.

(1) Holm, R. H. Iron-Sulfur Clusters. In *Bio-coordination Chemistry*; Que, L., Jr., Tolman, W. A., Eds.; Elsevier: Oxford, 2004; pp 61−90.
(2) Rao, P. V.; Holm, R. H. *Chem. Rev.* **2004**, *104*, 527–559.
(3) Koay, M. S.; Antonkine, M. L.; Gärtner, W.; Lubitz, W. *Chem. Biodiversity* **2008**, *5*, 1571–1587.
(4) Ogino, H.; Inomata, S.; Tobita, H. *Chem. Rev.* **1998**, *98*, 2093–2121.
(5) Angove, H. C.; Yoo, S. J.; Burgess, B. K.; Münck, E. *J. Am. Chem. Soc.* **1997**, *1997*, 8730–8731.
(6) Angove, H. C.; Yoo, S. J.; Münck, E.; Burgess, B. K. *J. Biol. Chem.* **1998**, *273*, 26330–26337.
(7) Yoo, S. J.; Angove, H. C.; Burgess, B. K.; Hendrich, M. P.; Münck, E. *J. Am. Chem. Soc.* **1999**, *121*, 2534–2545.
(8) Strop, P.; Takahara, P. M.; Chiu, H.-J.; Angove, H. C.; Burgess, B. K.; Rees, D. C. *Biochemistry* **2001**, *40*, 651–656.
(9) Hans, M.; Buckel, W.; Bill, E. *J. Biol. Inorg. Chem.* **2008**, *13*, 568–579.
(10) Goh, C.; Segal, B. M.; Huang, J.; Long, J. R.; Holm, R. H. *J. Am. Chem. Soc.* **1996**, *118*, 11844–11853.
(11) Zhou, H.-C.; Holm, R. H. *Inorg. Chem.* **2003**, *42*, 11–21.
(12) Scott, T. A.; Berlinguette, C. P.; Holm, R. H.; Zhou, H.-C. *Proc. Natl. Acad. Sci. U.S.A.* **2005**, *102*, 9741–9744.
(13) Deng, L.; Holm, R. H. *J. Am. Chem. Soc.* **2008**, *130*, 9878–9886.
(14) Münck, E.; Bominaar, E. L. *Science* **2008**, *321*, 1452–1453.
(15) Chakrabarti, M.; Deng, L.; Holm, R. H.; Münck, E.; Bominaar, E. L. *Inorg. Chem.* **2009**, *48*, 2735–2747.

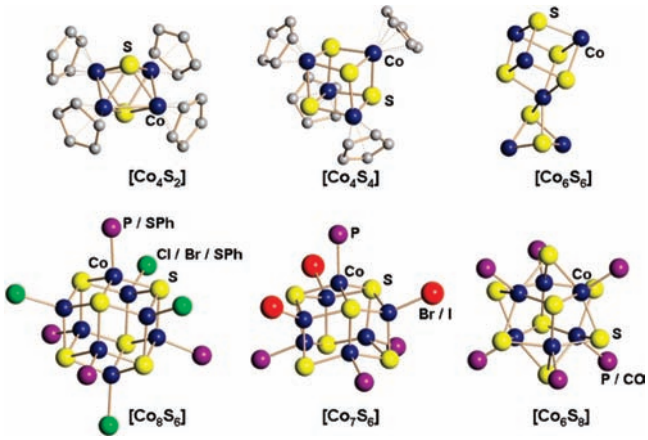

Figure 1. Structures of Co−S clusters with nuclearities of 4−8 showing the exclusive or usual terminal ligand atoms associated with each. The five η^5-C_5Me_5 ligands of Co_6S_6 are omitted for clarity.

variable M. The corresponding core units are unknown with other transition metals that manifest a tetrahedral stereochemical preference, necessitating synthesis of a new family of clusters. Cobalt(II) commonly exhibits this preference. However, we note that in the brief structural survey of Co−S clusters in Figure 1, which includes nuclearities $n = 4$,[16,17] 6,[18−22] 7,[23,24] and 8,[25] tetrahedral coordination is found only with $n = 7$ and 8, the large majority of the clusters are mixed-valence, and cubane stereochemistry is limited to a single example with Co^{III} ($[Cp_4Co_4S_4]$[17]). If Co−Se clusters are considered, different examples emerge that include the cubane $[Co_4Se_4(PPh_3)_4]$[26] and $[Co_8Se_8(PPh_3)_6]^{0,1+}$,[27] with a composition analogous to $[Fe_8S_8(PR_3)_6]$. In this investigation, we have prepared and structurally characterized the cubane-type clusters $[Co_4S_4(Pr^i{}_2NHCMe_2)_4]$ and $[Co_4S_4(PPr^i{}_3)_4]$, examined their redox chemistry, and determined magnetic ground states. As will be seen, these clusters exhibit an exchange coupling pattern and a highly paramagnetic ground state consonant with the properties of $[Fe_4S_4]^0$ clusters.

Experimental Section

Preparation of Compounds. All reactions and manipulations were performed under a pure dinitrogen atmosphere using either Schlenk techniques or an inert atmosphere box. Solvents were passed through an Innovative Technology or MBraun solvent purification system prior to use. Solvent removal steps were performed in vacuo. Selected compounds were analyzed (H. Kolbe, Mulheim, Germany). All compounds except $[Co(Pr^iNHCMe_2)_2Cl_2]$ were identified by X-ray structural determinations.

$[Co(Pr^i{}_2NHCMe_2)_2(SBu^t)_2]$. To a suspension of $CoCl_2$ (0.13 g, 1.0 mmol) in THF (10 mL) was added a solution of $Pr^i{}_2NHCMe_2$ (1,3-diisopropyl-4,5-dimethylimidazol-2-ylidene,[28] 0.36 g, 2.0 mmol) in THF (5 mL). The reaction mixture was stirred for 4 h. Addition of a solution of Bu^tSNa (0.22 g, 2.0 mmol) in THF (10 mL) resulted in formation of a green suspension. The mixture was stirred for 2 d and filtered. Vapor diffusion of *n*-hexane into the filtrate afforded the product as a green crystalline solid (0.43 g, 72%). Absorption spectrum (benzene): λ_{max} (ε_M) 344 (6820), 406 (2490), 456 (1460), 564 (353), 652 (1280), 717 (1144) nm. ^{1}H NMR (C_6D_6): δ 18.87 (12), 6.80 (9); (THF-d_8): δ 18.04 (12), 7.54 (9).

$[Co(Pr^i{}_2NHCMe_2)_2Cl_2]$. To a suspension of $CoCl_2$ (0.13 g, 1.0 mmol) in benzene (30 mL) was added a solution of $Pr^i{}_2NHCMe_2$ (0.36 g, 2.0 mmol) in THF (3 mL). The reaction mixture was stirred for 2 d. The blue suspension was filtered, and the solid was washed with ether (2 × 5 mL) and dried in vacuo. The product was obtained as a blue powder (0.44 g, 90%). Absorption spectrum (benzene): λ_{max} (ε_M) 312 (828), 597 (440), 640 (920) nm. ^{1}H NMR (C_6D_6): δ 14.63 (1), 8.78 (2).

$[Co_4S_4(PPr^i{}_3)_4]$. Method A of the preparation of $[Co_4S_4(Pr^i{}_2NHCMe_2)_4]$ (see below) was followed to the point of the brown oily residue, which was dissolved in THF (5 mL), and the solution was filtered. Layering acetonitrile (20 mL) on the filtrate caused separation of the product as black crystalline blocks (0.34 g, 70%). ^{1}H NMR (C_6D_6): δ 14.71 (1), 1.80 (6). Anal. Calcd: C, 43.03; H, 8.43; Co, 23.46; P, 12.33; S, 12.76. Found: C, 42.94; H, 8.39; Co, 23.49; P, 12.38; S, 12.77. A very small quantity of platelike black crystals was separated from the bulk product and shown to be $[Co_8S_8(PPr^i{}_3)_6]$ by an X-ray structure determination.

$[Co_4S_4(PPr^i{}_3)_4](BF_4)$. To a solution of $[Co_4S_4(PPr^i{}_3)_4]$ (0.19 g, 0.20 mmol) in THF (5 mL) was added $[Cp_2Fe](BF_4)$ (0.055 g, 0.20 mmol). The reaction mixture was stirred overnight. Solvent was removed, the deep brown residue was dissolved in acetonitrile (2 mL), and the solution was filtered. Vapor diffusion of ether into the brown filtrate afforded the product as deep brown blocklike crystals (0.15 g, 70%). Absorption spectrum (THF): λ_{max} (ε_M) 370 (sh, 13900) nm. ^{1}H NMR (CD_3CN): δ 2.65 (6), 2.32 (1). Anal. Calcd for $C_{36}H_{84}BCo_4F_4P_4S_4$: C, 39.60; H, 7.76; Co, 21.59; P, 11.35; S, 11.75. Found: C, 39.41; H, 7.49; Co, 22.19; P, 11.44. An accurate sulfur analysis was not obtained. A small amount of brown platelike crystals was also obtained from the bulk sample and shown by an X-ray structure determination to be $[Co_8S_8(PPr^i{}_3)_6](BF_4)$.

$[Co_4S_4(Pr^i{}_2NHCMe_2)_4]$. Method A. To a suspension of $CoCl_2$ (0.26 g, 2.0 mmol) and $PPr^i{}_3$ (0.64 g, 4.00 mmol)[29] in THF (10 mL) was added a solution of $(Me_3Si)_2S$ (0.43 g, 2.4 mmol) in THF (10 mL). The mixture was stirred for 2 d, solvent was removed, and the deep brown oily residue was dissolved in THF (10 mL). The solution was filtered. The filtrate was treated with a solution of $Pr^i{}_2NHCMe_2$ (0.72 g, 4.0 mmol) in THF (10 mL), resulting in a brown suspension, which was stirred for 7 d. The reaction mixture was filtered. Vapor diffusion of *n*-hexane into the brown filtrate afforded the product as a brown crystalline solid (0.28 g, 50%). ^{1}H NMR (C_6D_6): δ 7.37 (1), 5.38 (2), −11.6 (br). Anal. Calcd for $C_{44}H_{80}Co_4N_8S_4$: C, 48.70; H, 7.43; Co, 21.71; N, 10.33; S, 11.82. Found: C, 47.61; H, 7.29; Co, 21.23; N, 10.07; S, 11.53.

Method B. A solution of $[Co_4S_4(PPr^i{}_3)_4]$ (0.20 g, 0.20 mmol) in THF (5 mL) was treated with a solution of $Pr^i{}_2NHCMe_2$ (0.16 g, 0.90 mmol) in THF (5 mL). The reaction mixture was refluxed overnight and filtered. Solvent was removed from the filtrate, the deep brown oily residue was dissolved in benzene (5 mL), and the solution was filtered. Vapor diffusion of hexanes into the brown filtrate yielded the product as deep brown crystals (0.17 g, 80%).

(16) Jiang, F.; Lei, X.; Huang, Z.; Hong, M.; Kang, B.; Wu, D.; Liu, H. *J. Chem. Soc., Chem. Commun.* **1990**, 1655–1656.
(17) Simon, G. L.; Dahl, L. F. *J. Am. Chem. Soc.* **1973**, *95*, 2164–2174.
(18) Guo, S.; Hauptmann, R.; Losi, S.; Zanello, P.; Schneider, J. J. *J. Cluster Sci.* **2007**, *18*, 237–251.
(19) Cecconi, F.; Ghilardi, C. A.; Midollini, S.; Orlandini, A. *Polyhedron* **1986**, *5*, 2021–2031.
(20) Hong, M.; Huang, Z.; Lei, X.; Wei, G.; Kang, B.; Liu, H. *Polyhedron* **1991**, *10*, 927–934.
(21) Diana, E.; Gervasio, G.; Rossetti, R.; Valdemarin, F.; Bor, G.; Stanghellini, P. L. *Inorg. Chem.* **1991**, *30*, 294–299.
(22) Bencini, A.; Ghilardi, C. A.; Orlandini, A.; Midollini, S.; Zanchini, C. *J. Am. Chem. Soc.* **1992**, *114*, 9898–9908.
(23) Cecconi, F.; Ghilardi, C. A.; Midollini, S.; Orlandini, A. *Inorg. Chim. Acta* **1991**, *184*, 141–145.
(24) Jiang, F.; Huang, L.; Lei, X.; Liu, H.; Kang, B.; Huang, Z.; Hong, M. *Polyhedron* **1992**, *11*, 361–363.
(25) Christou, G.; Hagen, K. S.; Bashkin, J. K.; Holm, R. H. *Inorg. Chem.* **1985**, *24*, 1010–1018.
(26) Fenske, D.; Ohmer, J.; Hachgenei, J. *Angew. Chem., Int. Ed. Engl.* **1985**, *24*, 993–995.
(27) Fenske, D.; Ohmer, J.; Merzweiler, K. *Z. Naturforsch.* **1987**, *42b*, 803–809.
(28) Kuhn, N.; Kratz, T. *Synthesis* **1993**, 561–562.
(29) The compound $[Co(PPr^i{}_3)_2Cl_2]$ has been previously isolated: Allen, E. A.; Del Gaudio, J. *J. Chem. Soc., Dalton Trans.* **1975**, 1356–1360.

Chart 1. Designation of Compounds

$[Co(Pr^i_2NHCMe_2)_2X_2]$	X = Bu^tS^- **1**, Cl^- **2**
$[Co_4S_4(PPr^i_3)_4]$	**3**
$[Co_4S_4(PPr^i_3)_4]^+$	**4**
$[Co_4S_4(Pr^i_2NHCMe_2)_4]$	**5**
$[Co_4S_4(Pr^i_2NHCMe_2)_4]^+$	**6**
$[Co_8S_8(PPr^i_3)_6]$	**7**
$[Co_8S_8(PPr^i_3)_6]^+$	**8**
$[Fe_4S_4(Pr^i_2NHCMe_2)_4]$	**9**[13]
$[Fe_8S_8(Pr^i_2NHCMe_2)_6]$	**10**[13]
$[Fe_8S_8(PPr^i_3)_6]$	**11**[11]

The ^{1}H NMR spectrum of this material was identical with that of the product from Method A.

$[Co_4S_4(Pr^i_2NHCMe_2)_4](PF_6)$. To a solution of $[Co_4S_4(Pr^i_2NHCMe_2)_4]$ (0.11 g, 0.10 mmol) in THF (5 mL) was added $(C_7H_7)(PF_6)$ (0.024 g, 0.10 mmol). The mixture was stirred overnight. Solvent was removed, the deep brown residue was dissolved in THF (2 mL), and the solution was filtered. Vapor diffusion of *n*-hexane into the brown filtrate yielded the product as brown crystals (0.055 g, 40%). ^{1}H NMR (CD_3CN): δ 11.75 (1), 9.53 (2).

$[Co_4S_4(Pr^i_2NHCMe_2)_4](BPh_4)$. This compound was prepared on the same scale by the previous procedure but with use of $NaBPh_4$ (0.034 g, 0.10 mmol) in 5 mL of acetonitrile. Product was obtained as brown crystals (0.097 g, 70%) with an identical ^{1}H NMR spectrum of the cation. Absorption spectrum (THF): λ_{max} (ε_M) 374 (sh, 14100) nm.

In the sections that follow, compounds are referred to by the designations in Chart 1.

X-ray Structure Determinations. The structures of the seven compounds in supplemental Table S-1 in Supporting Information were determined. Diffraction-quality crystals were obtained as follows: **3** and **7**, THF/acetonitrile; **5**, benzene/hexane; [**4**](BF_4) and [**8**](BF_4), acetonitrile/ether; **1**, [**6**](BPh_4), THF/hexane. Crystallizations were performed at room temperature. Crystals were coated with Paratone-N oil and mounted on a Bruker APEX CCD-based diffractometer equipped with an Oxford low-temperature apparatus. Data were collected with scans of 0.3 s/frame for 30 s. Cell parameters were retrieved with SMART software and refined using SAINT software on all reflections. Data integrations were performed with SAINT, which corrects for Lorentz polarization and decay. Absorption corrections were applied using SADABS. Space groups were assigned unambiguously by analysis of symmetry and systematic absences determined by XPREP. All structures were solved and refined using SHELXTL. Metal and first coordination sphere atoms were located from direct-methods E-maps; other non-hydrogen atoms were found in alternating difference Fourier synthesis and least-squares refinement cycles and during final cycles were refined anisotropically. Hydrogen atoms were placed in calculated positions employing a riding model. Final crystal parameters and agreement factors are reported in Table S-1.[30] Three of the four PPr^i_3 ligands of **3** are each disordered over two positions with equal occupancies such that the two Co−P vectors of each site form angles of 19.1(1)°, 23.8(1)°, and 24.4(1)°.

Other Physical Measurements. All measurements were performed under anaerobic conditions. Absorption spectra were recorded with a Varian Cary 50 Bio spectrophotometer. ^{1}H NMR spectra were obtained with a Varian AM-400 spectrometer. Cyclic voltammetry measurements were made with a BioAnalytical Systems Epsilon potentiostat/galvanostat in THF solutions using a sweep rate of 100 mV/s, a glassy carbon working electrode, 0.1 M $(Bu_4N)(PF_6)$ supporting electrolyte, and an SCE reference electrode. Under these conditions, $E_{1/2}$ = 0.55 V for the $[Cp_2Fe]^{0,1+}$ couple.

(30) See paragraph at the end of this article for Supporting Information available.

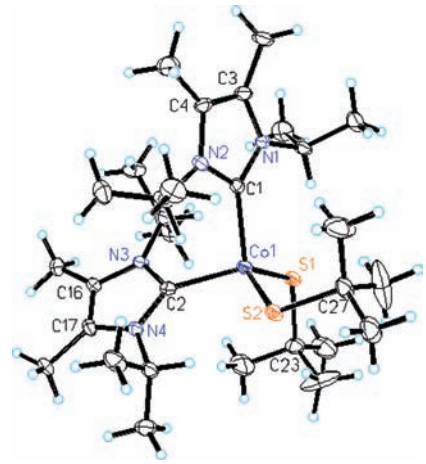

Figure 2. Structure of $[Co(Pr^i_2NHCMe_2)_2(SBu^t)_2]$ showing 50% probability ellipsoids and the atom labeling scheme. Selected values: Co−C 2.085[1] Å, Co−S 2.287[1] Å, S1−Co−S2 116.66(6)°, C1−Co−C2 103.1(2)°, C1−Co−S1 112.1(2)°, C1−Co−S2 106.5(2)°, C2−Co−S1 106.0(2)°, C2−Co−S2 111.7(2)°.

Magnetic susceptibility data were obtained with powder samples at 2−300 K using a SQUID susceptometer with a field of 1.0 T (MPMS-7, Quantum Design, calibrated with a palladium reference sample, error < 2%). Multiple-field variable-temperature measurements were done at 1, 4, and 7 T also at 2−300 K with the magnetization sampled in equidistant steps on a 1/*T* temperature scale. The data were corrected for diamagnetic contributions by using Pascal's constants,[31] as well as for temperature-independent paramagnetism. The susceptibility and magnetization data for the cluster compounds were simulated using the usual spin-Hamiltonian operator 1 for a system of four high spin Co(II) sites with local spin $S_i = 3/2$. Here $J_{i,j}$ are the isotropic coupling constants for the exchange interaction between the individual cobalt ions (i = 1, 4), g_i are the average electronic *g*-values, and D_i and E/D_i are the average zero-field splitting and rhombicity parameters for the ions. Alternatively, the data for the cluster compounds were also simulated using the total spin S_t of the ground state only in conjunction with the usual Hamiltonian operator 2 for a single spin S where S was set to S_t and $g = g_t$, $D = D_t$, and $E/D = (E/D)_t$. For mononuclear complexes, the usual spin-Hamiltonian operator 2 for $S = 3/2$ was used. Simulations were done with our own package julX for exchange-coupled systems.[32] The values were summed over a 16-point Lebedev grid[33,34] to account for the powder distribution with respect to the field. For some samples, intramolecular interactions were taken into account in the simulations by using a Weiss temperature Θ_W as a perturbation of the temperature scale, $kT' = k(T - \Theta_W)$.

$$\hat{H} = -2\sum_{j<i} J_{i,j}\hat{\vec{S}}_i\cdot\hat{\vec{S}}_j + \sum_i g_i\beta\hat{\vec{S}}_i\cdot\vec{B} + \sum_i D_i[\hat{S}_{i,z}^2 - 5/4 + E/D_i(\hat{S}_{i,x}^2 - \hat{S}_{i,y}^2)] \quad (1)$$

$$\hat{H} = g\beta\hat{\vec{S}}\cdot\vec{B} + D[\hat{S}_z^2 - 1/3S(S+1) + E/D(\hat{S}_x^2 - \hat{S}_y^2)] \quad (2)$$

Results and Discussion

Mononuclear Complexes. In seeking clusters with the cubane-type $[Co_4S_4]$ core unit, we note stabilization of $[Co_4Se_4]$ species

(31) O'Connor, C. J. *Prog. Inorg. Chem.* **1982**, *29*, 203–283.
(32) Available through http://ewww/mpi-muelheim.mpg.de/bac/logins/bill/julX_en.php.
(33) Lebedev, V. I.; Laikov, D. N. *Dokl. Math.* **1999**, *59*, 477–481.
(34) A Fortran code to generate Lebedev grids up to order L = 131 is available at http//:server.ccl.net/cca/software/SOURCES/.

by tertiary phosphines[26] as well as reduced $[Fe_4S_4]^{0,1+}$ clusters by phosphine[10,11] and *N*-heterocyclic carbene[13] terminal ligation. Anionic ligands such as thiolate increase cluster negative charge and promote oxidative instability. Mononuclear Co(II) phosphine complexes, many of the tetrahedral type $[Co(PR_3)_2L_2]$, abound. While carbene complexes of the divalent ions Fe^{II}, Ni^{II}, Pd^{II}, and Pt^{II} have been extensively investigated in this decade,[35−37] recent work on Co^{II} carbenes has largely utilized tripodal ligands favoring tetrahedral stereochemistry.[38,39] We wished to ascertain whether carbenes would be effective in stabilizing unconstrained high-spin tetrahedral Co^{II} resembling sites in a cubane-type cluster. The complexes $[Co(Pr^i_2NHCMe_2)_2(SBu^t)_2]$ and $[Co(Pr^i_2NHCMe_2)_2Cl_2]$ are readily prepared. The structure of **1**, shown in Figure 2, reveals tetrahedral stereochemistry with bond angles in the range 106−117°, normal Co−S bond lengths when compared to other tetrahedral $[Co(SR)_2L_2]$ complexes (2.24−2.27 Å),[40,41] and Co−C bond lengths the same as or at most ca. 0.05 Å longer than those in other tetrahedral Co^{II} carbenes.[38,39] In benzene solution, the complexes exhibit visible ligand field bands of tetrahedral ($^4A_{2g} \rightarrow {}^4T_{1g}(P)$) parentage at energies similar to those observed for $[Co(SR)_2L_2]$ species.[41]

The temperature dependencies of the magnetic moments of complexes **1** and **2** were determined at 2−300 K. Above 150 K, both exhibit constant moments of ca. 4.2 μ_B, which is close to the spin-only value of 3.87 μ_B ($g = 2$) for $S = 3/2$. Below 150 K, magnetic moments of both compounds increase and reach maxima near 10 K, a behavior typical of intermolecular ferromagnetic spin coupling. The full temperature dependencies could be reasonably well simulated with $S = 3/2$, $g = 2.180$, and $\Theta_W = +0.8$ K for **1** and $g = 2.186$ and $\Theta_W = +1.2$ K for **2**.[30] Reliable values for zero-field splitting parameters, however, could not be determined because of the effects of intermolecular interactions. A rough upper limit of $|D| < 5$ cm^{-1} could be estimated from systematic variations of D and Θ_W in the simulations. These results show that when paired with conventional ligands the carbene, like phosphines, behaves as a normal weak field ligand that stabilizes tetrahedral Co^{II} in the absence of any ligand-imposed structural preference. Both ligand types were utilized in cluster synthesis.

Cubane-Type Clusters. (a) Neutral Clusters. Synthetic methods are summarized in Figure 3. Phosphine cluster **3** is obtained by self-assembly reaction 3. Carbene cluster **5** is also prepared by self- assembly. In that system, **3** is first formed and subjected in situ to ligand displacement reaction 4 by the addition of excess $Pr^i_2NHCMe_2$. Alternatively, preisolated **3** is treated with a small excess of carbene to afford **5**. Both methods lead to essentially the same yield of isolated product (ca. 50−60%). Analogous iron−sulfur carbene cluster **9** is also prepared in a similar self-assembly system but with the intermediate formation of edge-bridged double cubane **10**[13] (see below). No intermediate was encountered in the preparation of **5** by self-assembly. However, in the preparation of **3** by reaction 3, a very small amount of a black crystalline byproduct was obtained. Its composition was established as $[Co_8S_8(PPr^i_3)_6]$, comparative to **11**, by an X-ray structure determination. As will be seen, the structures of clusters **7** and **11** are not the same. Reactions 4 and 5[13] provide a clear demonstration of the stronger binding affinity of a carbene versus trialkylphosphine toward a common site, here tetrahedral Fe^{II} or Co^{II}.

$$4[Co(PPr^i_3)_2Cl_2] + 4(Me_3Si)_2S \rightarrow [Co_4S_4(PPr^i_3)_4] + 8Me_3SiCl + 4PPr^i_3 \quad (3)$$

$$[Co_4S_4(PPr^i_3)_4] + 4Pr^i_2NHCMe_2 \rightarrow [Co_4S_4(Pr^i_2NHCMe_2)_4] + 4PPr^i_3 \quad (4)$$

$$[Fe_8S_8(PPr^i_3)_6] + 8Pr^i_2NHCMe_2 \rightarrow 2[Fe_4S_4(Pr^i_2NHCMe_2)_4] + 6PPr^i_3 \quad (5)$$

The structures of **3** and **5**, set out in Figures 4 and 5, respectively, reveal the desired cubane-type stereochemistry with similar core dimensions as evident from the metric information in Table S-2 in Supporting Information. The Co^{II} sites have trigonally distorted tetrahedral stereochemistry. In cluster **5**, the mean Co−C bond lengths are ca. 0.1 Å longer than in mononuclear **1**, owing to steric interactions with the bulky carbene and thiolate ligands.

The Co_4S_4 cores approach T_d symmetry; no systematic deviations from that symmetry are evident. The structural similarity between **3** and **5** and their close relationship to iron−sulfur cluster **9** is emphasized by the comparisons of mean distances and volumes calculated from atomic coordinates[42] in Table 1. The cause of the 0.09 Å longer mean Co−Co distance and correspondingly larger Co_4 and Co_4S_4 volumes in **3** compared to **5** is unclear. The longer mean Fe−S bond length and larger S_4 and Fe_4S_4 volumes in **9** versus the cobalt clusters arise from the difference of 0.05 Å in Shannon radii[43] between tetrahedral Fe^{II} and Co^{II}.

(b) Redox Series and Oxidized Clusters. Voltammograms of THF solutions prepared from the two neutral clusters are presented in Figure 6. Each supports two quasireversible processes, a reduction and oxidation for **3** and two oxidations for **5**. The latter showed no reduction out to −2.0 V. The data are summarized and compared with the behavior of iron cluster **9**[13] and $[Fe_4S_4(PPr^i_3)]^{1+1}$[11] in Figure 7. Two trends in the redox couples are defined by decisively large potential differences: $E_{Fe}^{0/1+} < E_{Co}^{0/1+}$ at constant ligand and $E_{carbene}^{0/1+;1+/2+} < E_{phosphine}^{0/1+;1+/2+}$ at constant metal. The first trend has one precedent with cubane (Fe_4S_4, $CoFe_3S_4$) clusters.[44] The second and more significant trend implies that carbene is a more effective σ-donor to the core, resulting in a greater ease of electron loss. This statement is consistent with previous evidence that carbenes are more effective electron donors than the more basic phosphine ligands,[45−47] We are unaware of other quantitative data bearing on the comparative redox potentials of carbene and phosphine ligation.

(35) Herrmann, W. A. *Angew. Chem., Int. Ed.* **2002**, *41*, 1290–1309.
(36) Crudden, C. M.; Allen, D. P. *Coord. Chem. Rev.* **2004**, *248*, 2247–2273.
(37) Hahn, F. E.; Jahnke, M. C. *Angew. Chem., Int. Ed.* **2008**, *47*, 3122–3172.
(38) Hu, X.; Castro-Rodriguez, I.; Meyer, K. *J. Am. Chem. Soc.* **2004**, *126*, 13464–13473.
(39) Cowley, R. E.; Bontchev, R. P.; Duesler, E. N.; Smith, J. M. *Inorg. Chem.* **2006**, *45*, 9771–9779.
(40) Corwin, D. T., Jr.; Gruff, E. S.; Koch, S. A. *J. Chem. Soc., Chem. Commun.* **1987**, 966–967.
(41) Corwin, D. T., Jr.; Fikar, R.; Koch, S. A. *Inorg. Chem.* **1987**, *26*, 3080–3082.
(42) Kaspar, J. S.; Lonsdale, K. In *International Tables for X-Ray Crystallography*; Kynoch: Birmingham, U. K., 1967; pp 36−49.
(43) Shannon, R. D. *Acta Crystallogr.* **1976**, *A32*, 751–767.
(44) Zhou, J.; Raebiger, J. W.; Crawford, C. A.; Holm, R. H. *J. Am. Chem. Soc.* **1997**, *119*, 6242–6250.
(45) Huang, J.; Schanz, H.-J.; Stevens, E. D.; Nolan, S. P. *Organometallics* **1999**, *18*, 2370–2375.
(46) Perrin, L.; Clot, E.; Eisenstein, O.; Loch, J.; Crabtree, R. H. *Inorg. Chem.* **2001**, *40*, 5806–5811.

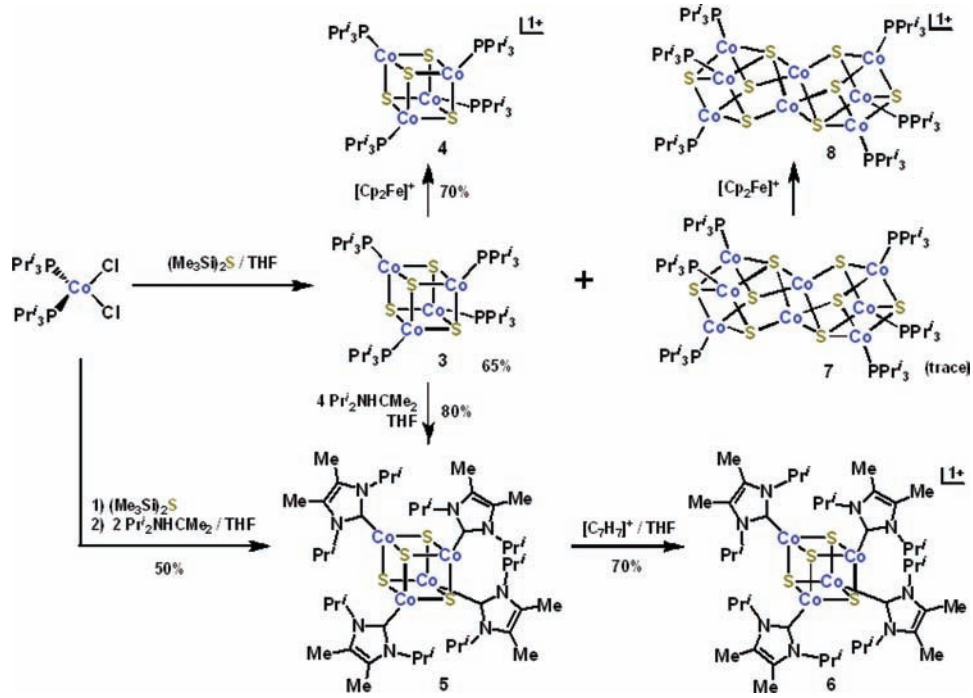

Figure 3. Scheme for the preparation of phosphine clusters **3**, **4**, **7**, and **8** and carbene clusters **5** and **6**. Clusters **7** and **8** were obtained in low yields as reaction byproducts.

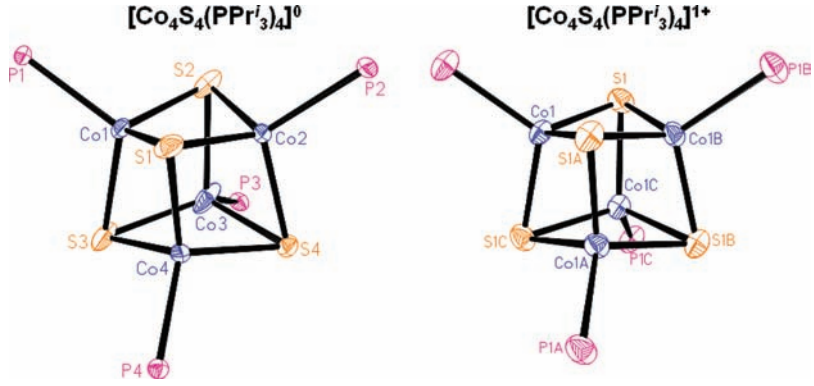

Figure 4. Structures of $[Co_4S_4(PPr^i_3)_4]^{0,1+}$ showing 30% probability ellipsoids and the atom numbering schemes. Ligands P(1,3,4)Pr^i_3 of the neutral cluster are disordered over two positions (not shown). The cation has crystallographically imposed T_d symmetry. Isopropyl groups are omitted for clarity.

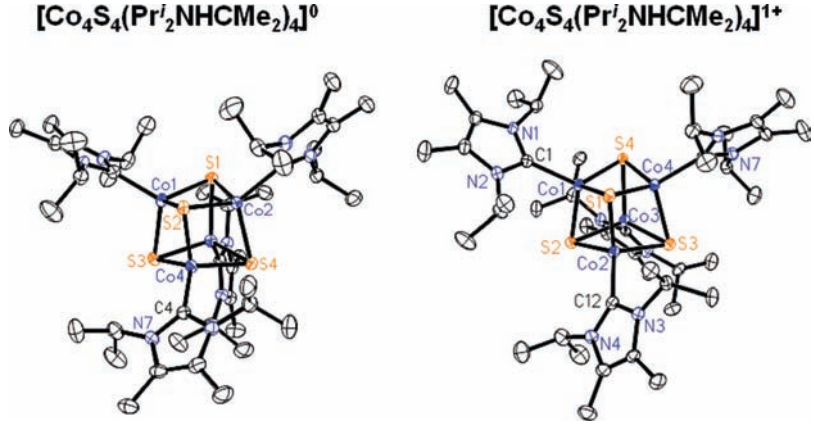

Figure 5. Structures of $[Co_4S_4(Pr^i_2NHCMe_2)_4]^{0,1+}$ showing 30% probability ellipsoids and the atom numbering schemes.

Clusters **3** and **5** are readily oxidized to monocations **4** and **6** by ferrocenium and tropylium ions, respectively, and isolated as crystalline salts. Their structures retain the cubane-type geometry (Figures 4 and 5) with dimensions similar to those of the neutral clusters. While these reactions lead to formal mixed-valence ($3Co^{II} + Co^{III}$) cores, the metric parameters in Table

Table 1. Summary of Core Structural Comparisons of Cubane-Type Clusters $[M_4S_4L_4]^{0,1+}$ (M = Co, Fe; L = PPr^i_3, $Pr^i_2NHCMe_2$)

cluster	M−S (Å)[a]	M−M (Å)[a]	$V(M_4)$ (Å^3)[b]	$V(S_4)$ (Å^3)	$V(M_4S_4)$ (Å^3)
$[Co_4S_4(PPr^i_3)_4]$[c]	2.223[8]	2.603[9]	2.08	5.26	8.50
$[Co_4S_4(Pr^i_2NHCMe_2)_4]$[d]	2.25[1]	2.69[2]	2.30	5.33	9.12
$[Fe_4S_4(Pr^i_2NHCMe_2)_4]$[e,f]	2.33[2]	2.68[1]	2.26	6.14	9.47
$[Co_4S_4(PPr^i_3)_4]^{1+}$[f]	2.206(1)	2.607(1)	2.10	5.06	8.44
$[Co_4S_4(Pr^i_2NHCMe_2)_4]^{1+}$[g]	2.22[1]	2.66[2]	2.22	5.06	8.77

[a] Mean values. [b] Volume calculations: ref 43; Shannon tetrahedral crystal radii (Å): Fe^{II} = 0.77, Co^{II} = 0.72. [c] 130 K. [d] 105 K. [e] Reference 13, 193 K. [f] 193 K. [g] 100 K.

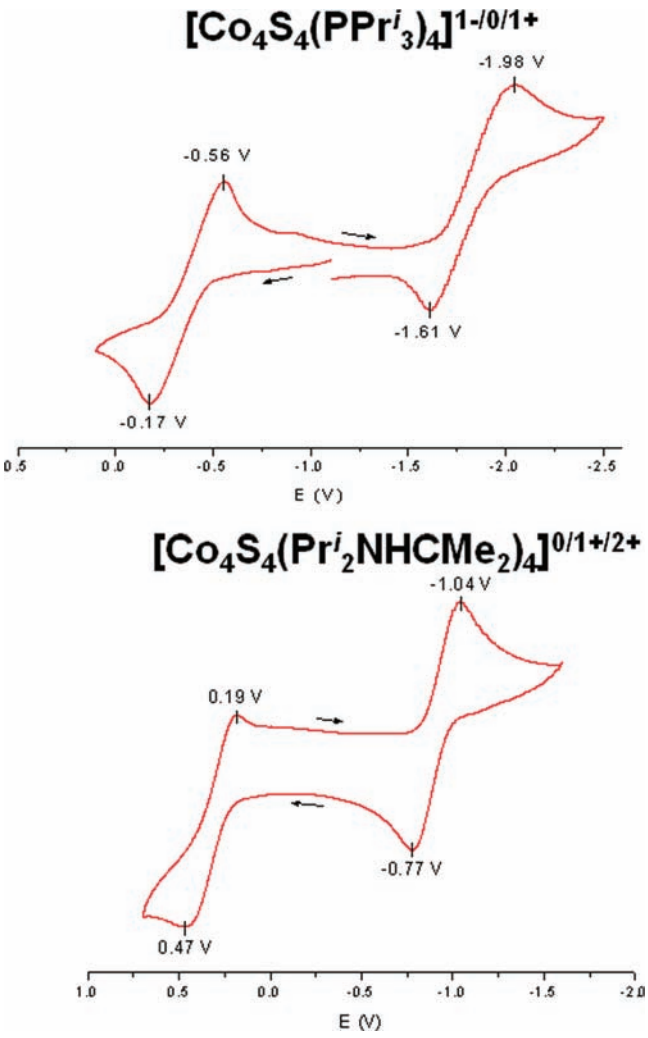

Figure 6. Cyclic voltammograms (100 mV/s) of ca. 3 mM THF solutions prepared from $[Co_4S_4(PPr^i_3)_4]$ (upper) and $[Co_4S_4(Pr^i_2NHCMe_2)_4]$ (lower). Peak potentials versus SCE are indicated.

S-3[30] in Supporting Information provide no distinction in metal sites and thus suggest electron delocalization in the $[Co_4S_4]^{1+}$ core or disorder. The small decreases in S_4 and Co_4S_4 volumes imply (but do not prove) removal of an electron from an antibonding orbital with substantial sulfur character.

(c) Magnetic Ground States. The temperature dependence of the effective magnetic moment of carbene cluster **5**, depicted in Figure 8, steeply increases from 4.7 μ_B at 2 K to 6.7 μ_B at 10 K, which persists up to about 100 K. The moment then decreases, reaching 5.2 μ_B at 300 K. These large magnetic moments are not necessarily expected because a simple analysis of a symmetic $[Co_4S_4]^0$ core with equal exchange couplings between metal sites predicts a diamagnetic ground state (S_t = 0). In contrast, the value observed for **5** at 10−100 K is close to the spin-only value $\mu_{so} = 2(3\cdot4)^{1/2} = 6.93\ \mu_B$ for $S = 3$. Accordingly, a preliminary simulation with $S_t = 3$ and g_t = 1.936 (dashed line) provides a good approximation to the experimental data up to about 100 K, including the decline of μ_{eff} below 10 K where the effect appears to be due to field saturation. Above 120 K the simple model fails, apparently because manifolds with $S_t < 3$ become populated. The low average g-value used in the approximate treatment is remarkable because Co^{II}, with a more than half-filled d-shell ($3d^7$), should have $g > 2$. This matter is discussed below.

The magnetic data for phosphine cluster **3** in Figure 9 reveals $\mu_{eff} \approx 6.6\ \mu_B$ at 10−100 K, similar to the behavior of **5**. The maximum at lower temperatures is indicative of intermolecular interactions, and the values above 100 K decrease much less than those of **5**. The latter behavior indicates a different extent of spin coupling for the two clusters and a higher separation of excited spin states for **3**. The ground state spin $S_t = 3$ was corroborated by multifield magnetization measurements and data fits. Nesting of the isofield magnetization curves at B = 1, 4, and 7 T is consistent only with a spin septet with weak zero-field splitting, although it proved difficult to simulate accurately the entire data set because of intermolecular interactions. The data at 4 and 7 T approach saturation close to $M_{mol}/Ng\mu_B = 3$, expected for $S_t = 3$ with $g = 2$. The deviation suggests a lower g-value for the ground state, as found in simulations.

The paramagnetism of **3** and **5** is reminiscent of the situation with $[Fe_4S_4]^0$ clusters of the iron protein of *Av* nitrogenase,[7] the dehydratase activator protein,[9] and synthetic cluster **9**.[13−15] The four Fe^{II} sites are exchange-coupled via four μ_3-S bridges such that the local spins $S_{Fe} = 2$ yield $S_t = 3\cdot2 - 2 = 4$ for the cluster ground state. It has been observed that the all-ferrous clusters must have lower than cubic symmetry and the distortion appears to stabilize the highly reduced system.[14,15] Spectroscopic asymmetry first became evident in the Mössbauer spectrum of the *Av* iron protein, which showed two resolved quadrupole doublets in the 3:1 intensity ratio with distinct quadrupole and magnetic hyperfine couplings.[5] The spin of one Fe^{II} site is aligned opposite to those of the other three sites. The same 3:1 pattern is found with the activator protein and synthetic cluster.

Although we do not have positive indication of a 3:1 site core geometric distortion in **3** and **5** and hyperfine measurements are elusive for these integer spin systems, we assume the same spin topology.[48] The 3:1 spin-coupling scheme readily rationalizes the ground state of $[Co_4S_4]^0$ cores with $S_{Co} = 3/2$: $S_t = 3(3/2) - 3/2 = 3$. Corresponding spin Hamiltonian simulations yield convincing results for the low temperature magnetic data of **5** (Figure 8). Two independent coupling constants have been used to model in the antiferromagnetic interaction of three similar and one different metal site. The observed spin arises from the antiparallel orientation of site (1) relative to sites (2−4) when J-coupling exceeds J'-coupling.

(47) Chianese, A. R.; Li, X.; Janzen, M. C.; Faller, J. W.; Crabtree, R. H. *Organometallics* **2003**, *22*, 1663–1667.

(48) In view of the magneto-elastic coupling found for all-ferrous **9**,[15] we assume that the dependencies of the exchange coupling constants and symmetry-breaking deformations ($(dJ/dr)\Delta r$) may be stronger for the cobalt than iron clusters, such that small deformations already afford sizeable changes in exchange energy. Additionally, the unique spin site (1 in Figure 8) may be disordered in the crystalline state.

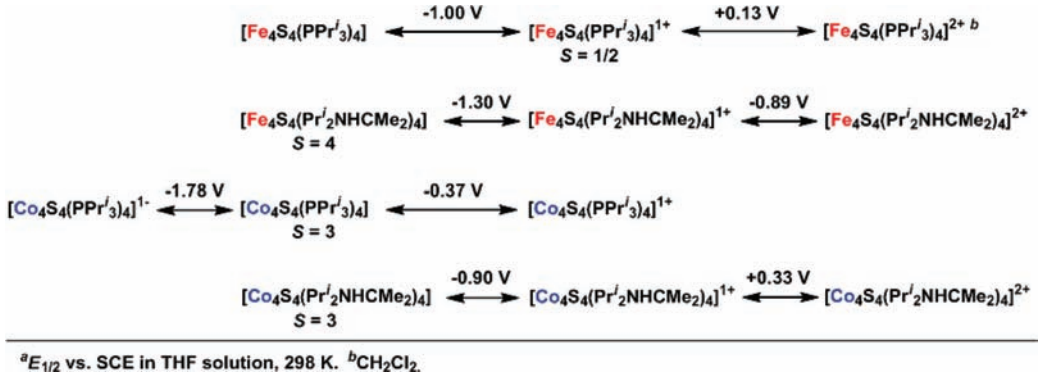

Figure 7. Summary of redox reactions of $[M_4S_4(PPr^i_3)_4]$ and $[M_4S_4(Pr^i_2NHCMe_2)_4]$ (M = Fe, Co) in THF solutions showing $E_{1/2}$ values versus SCE. The potential of the top reaction refers to dichloromethane solution.

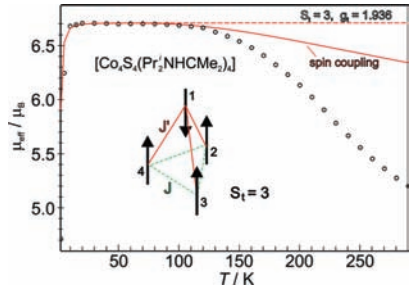

Figure 8. Temperature dependence of the effective magnetic moment of solid $[Co_4S_4(Pr^i_2NHCMe_2)_4]$ measured at applied field $B = 1$ T. The dashed line is a preliminary simulation with $S = 3$, $g = 1.936$, and $D = 0$. The solid line represents a generic spin Hamiltonian simulation with four spins: $S_i = 3/2$, $i = 1-4$, arranged in pyramidal topology with one unique site (spin 1) and two different exchange coupling constants $J = -420$ cm^{-1} for the interactions (1−2), (1−3), and (1−4), and $J' = -100$ cm^{-1} for (2−3), (3−4), and (4−2). Other parameters are $g_1 = 2.17$, $g_{234} = 2.0$, and $D_i = 0$. Inset: spin-coupling scheme for the $S_t = 3$ ground state.

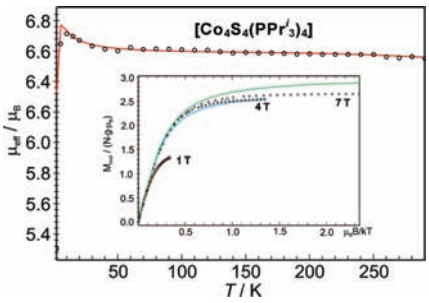

Figure 9. Temperature dependence of the effective magnetic moment of solid $[Co_4S_4(PPr^i_3)_4]$ measured at applied field $B = 1$ T. The solid line represents a generic spin Hamiltonian simulation with four spins: $S_i = 3/2$, $i = 1-4$, arranged in pyramidal topology with one unique site (spin 1) and two different exchange coupling constants $J = -600$ cm^{-1} for the interactions (1−2), (1−3), and (1−4), and $J' = -100$ cm^{-1} for (2−3), (3−4), and (4−2). Other parameters are $g_1 = 2.27$, $g_{234} = 2.0$, $D_i = 0$, $\Theta_W = 0.7$ K. Inset: multifield variable-temperature measurement of magnetization. The solid lines represent spin Hamiltonian simulations obtained with $S_t = 3$, $g_t = 1.90$, $D_i = -1.95$, $E/D_i = 0.2$, $\Theta_W = 0.7$ K.

While the magnetic data firmly establish the $S_t = 3$ ground state for clusters **3** and **5,** certain limitations in the analyses presented in Figures 8 and 9 are noted. The specified coupling constants are not unique. Many other J/J' combinations yield virtually the same result including the decrease in moment of **5** above 120 K. Apparently, we cannot observe or resolve a sufficient number of excited states to arrive at a unique fit. The lower part of the spin energy spectrum computed using the parameters for the spin Hamiltonian simulation for **5** consists

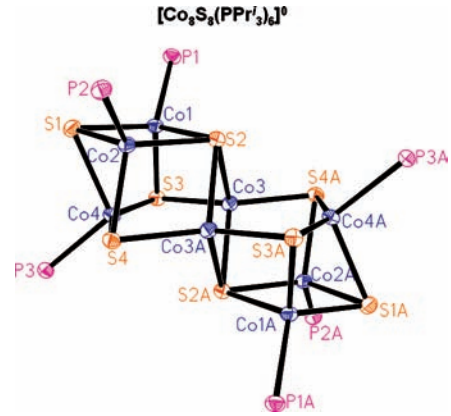

Figure 10. Structure of $[Co_8S_8(PPr^i_3)_6]$ showing 30% probability ellipsoids and the atom numbering scheme. The cluster has crystallographically imposed centrosymmetry. Isopropyl groups are omitted for clarity. Selected interatomic distances (A) and angles (deg): Co−(μ_3-S), 2.21[4]; Co−(μ_4-S), 2.24[1]; Co−Co, 2.59[7]; Co3−Co4, 2.952(1); Co3A−Co4, 2.913(1); Co−P, 2.24[1]; S2−Co3−S2A, 110.19(3); Co3−S2−Co3A, 69.81(3).

of a sequence of septet, quintet, triplet, and singlet states (Figure S-3A, Supporting Information).[30] The corresponding Boltzman population of the lowest manifolds (Figure S-3B, Supporting Information) qualitatively explains the decrease in μ_{eff} above 120 K as the onset of thermal population of the first excited spin quintet. However, we were unable to find satisfactory combinations of coupling constants J_{ij} that would shift the triplet and singlet states sufficiently close to the ground state to improve the fit. The virtually constant moment of **3** at 10−300 K indicates exclusive population of the spin septet state over that temperature interval. While this behavior constrains the possible J/J' values, a unique solution is not possible. The values given for J and J' (Figure 9) exemplify those required for a satisfactory fit.[49]

In the context of the spin coupling scheme, the low g-values of the $S_t = 3$ ground state derive mainly from the negative contribution of the unique site (1) with respect to the other three if $g_1 > 2$ supersedes the positive contributions g_{234} to g_t from the other sites. Because S_1 is oriented antiparallel to the total spin, the basic spin projection scheme of the fictitious intermediate spin $S_{234} = 9/2$ formed by the parallel arrangement of S_2, S_3, and S_4 and the unique site S_1 yields for the resulting total spin $g_t = -3/8g_1 + 11/8g_{234}$. Here g_{234} is the same as the g-value of each Co^{II} at sites 2, 3, and 4. In the simulation for **5**, we obtained the correct (observed) value $g_t = 1.936$ with $g_1 = 2.17$ and $g_{234} = 2$, and for **3** $g_t = 1.90$ with $g_1 = 2.27$ and $g_{234} = 2$. Again, the choice of values is not unique, but those given

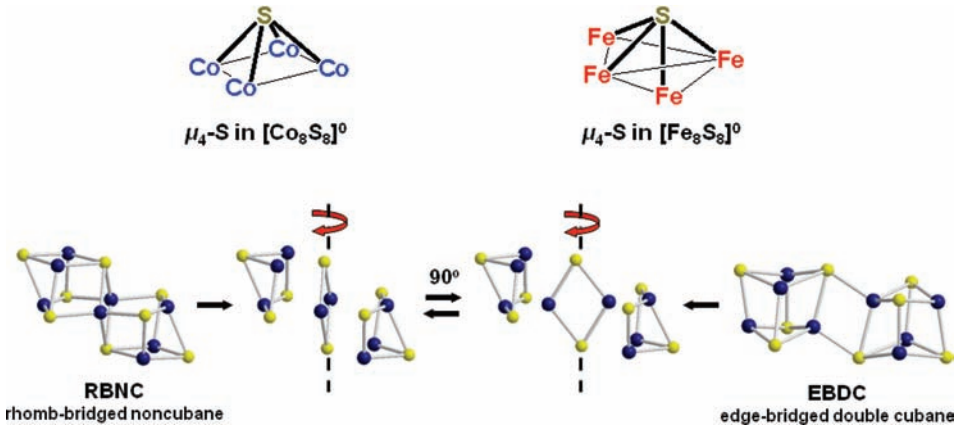

Figure 11. Conceptual topological transformation between a rhomb-bridged noncubane (RBNC) and edge-bridged double cubane (EBDC) structures of clusters with $[M_8S_8]$ cores.

demonstrate that the experimental data are consistent with the site values $g_{Co} > 2$.

Octanuclear Clusters. As noted above, phosphine cluster **7** was separated manually in small amounts in the synthesis of **3** by self-assembly. Its structure, which has imposed centrosymmetry, is provided in Figure 10. The $[Co_8(\mu_3\text{-}S)_6(\mu_4\text{-}S)_2]$ core is not built of cubane units. Two Co_3S_3 fragments (Co(1,2,4)S(1,3,4) and its symmetry equivalent) are bridged by a total of four Co-(μ_4-S) and four Co-(μ_3-S) interactions to an interior Co(3,3A)S(2,2A) rhomb with dimensions Co−S 2.250[3] Å, Co−Co 2.575(1) Å, S−Co−S 69.81(3)°, and Co−S−Co 110.19(3)°. The Co_8 part of the structure may be visualized as two Co_5 square pyramids sharing an edge (Co3−Co3A)with two apical Co atoms (Co4, Co4A) on opposite sites of the two basal planes which are themselves coplanar. Also identifiable are two Co_4S square pyramids with the same common edge and oppositely placed apical μ_4-S(2,2A) atoms. All Co sites are four-coordinate and approach tetrahedral stereochemistry. Atoms Co(3,3A) show the most pronounced deviation, with one large angle S3−Co3−S4A = 133.87(3)°; other angles at these atoms are in the 100.6−110.2° range.

Similarly, in the preparation of cation cluster **4**, the compound [**8**](BF_4) was obtained as a byproduct in minor amounts. The structure of the cation (not shown) is nearly indistinguishable from that of **7**, and there is no evidence of a discrete Co^{III} site. Further structural details on **7** and **8** are available.[30] These structures are precedented only by the compounds $[Co_8Se_8(PPh_3)_6][CoCl_3(PPh_3)]$ and $[Co_8Se_8(PPh_3)_6][Co_6Se_8(PPh_3)_6]$ originating from the reaction of $[CoCl_3(PPh_3)]^{1-}$ and $(Me_3Si)_2Se$.[27]

Although we have not been able to devise a synthetic method for which **7** is the principal product, we present this cluster here because of our interest in and utilization of Fe_8S_8 double cubane clusters in the preparation of other high-nuclearity clusters. Evidently, for $[M_8S_8]$ cores with tetrahedral sites *there are at least two structural solutions*, the edge-bridged double cubane (EBDC) and the rhomb-bridged noncubane (RBNC). The present examples of these structures are topological isomers. When considered in terms of core valence electron count, stable homometallic structures are currently restricted to 119−120 e^- for RBNC (**7**, **8**) and 110−112 e^- for EBDC (**10**, **11**, $[Fe_8S_8(PPr^i_3)_4(SSiPh_3)_2]$[11]).[50] This observation suggests that the two structures might be of competitive energy somewhere in between these limits. We note the conceptual least-motion RBNC ↔ EBDC interconversion of Figure 11. Proceeding from RBNC, cluster deconstruction affords two M_3S_3 fragments and the interior rhomb. Rhomb rotation by 90° around the S−S axis and recombination with the trinuclear fragments generates the EBDC. The process in effect converts two square pyramidal M_4S entities in the original structure to two trigonal bipyramidal M_4S substructures The cluster core $[Fe_4Co_4S_8]$, if synthetically accessible with tolerably small dimensional differences (Table 1), is one candidate with which to address the issue of relative stability of these two structures.

Conclusions

The following are the principal results and conclusions of this investigation:

(1) The assembly system $CoCl_2/Pr^i_3P/(Me_3Si)_2S$ in THF affords the cluster $[Co_4S_4(PPr^i_3)_4]$, which upon reaction with the carbene $Pr^i_2NHCMe_2$ yields $[Co_4S_4(Pr^i_2NHCMe_2)_4]$. These compounds can be oxidized to monocations by reactions with ferrocenium or tropylium. These species are the first examples of $[M_4S_4L_4]^z$ clusters with cubane-type stereochemistry, tetrahedral M sites, and a transition metal other than iron.

(2) The clusters in (1) are essentially isostructural with one another and with $[Fe_4S_4(Pr^i_2NHCMe_2)_4]$. Small dimensional differences between the cobalt and iron carbene cluster are mainly due to differences in M^{II} radii. Structures of mixed-valence cation clusters do not reveal electronically localized sites.

(3) Ligand substitution of phosphine by carbene in (1) and with iron clusters[13] and lower redox potentials for the 0/1+ and 1+/2+ couples of carbene versus phosphine clusters at constant metal are consistent with carbene being the better electron donor, at least to tetrahedral Co^{II} and Fe^{II}.

(4) $[Co_4S_4(PPr^i_3)_4]$ and $[Co_4S_4(Pr^i_2NHCMe_2)_4]$ have $S_t = 3$ ground states,[51] which may be rationalized in terms of coupling among three parallel and one antiparallel $S = 3/2$ spins of the Co^{II} sites. This 3:1 pattern of spin-coupling applies also to

(49) The slight slope in the data above 50 K results from intermolecular interactions described by $\Theta_W = -0.7$ K to account for the low temperature maximum in the fit and not from thermal population of an excited state.

(50) Given the existence of $[Mo_2Fe_6S_8]^{4+}$ and $[V_2Fe_6S_8]^{2+}$ clusters, the lower limit for the EBDC structure when isolated heterometallic clusters are included is presently 104 e^-: Osterloh, F.; Segal, B. M.; Achim, C.; Holm, R. H., *Inorg. Chem.* **2000**, *39*, 980–989. Hauser, C.; Bill, E.; Holm, R. H. *Inorg. Chem.* **2002**, *41*, 1615–1624.

(51) Theses results suggest a reexamination of the magnetism of $[Co_4Se_4(PPh_3)_4]$, which is reported to be diamagnetic.[26]

$[Fe_4S_4(Pr^i{}_2NHCMe_2)_4]$, whose $S_t = 4$ ground state motivated this investigation. A theoretical model of the origin of the spin-coupling scheme for the cobalt clusters is not yet available. A model based on spontaneous distortions of the $[Fe_4S_4]^0$ core has been recently described.[15]

(5) The $[Co_8S_8]^0$ core of $[Co_8S_8(PPr^i{}_3)_6]$, obtained as a minor byproduct in the synthesis of $[Co_4S_4(PPr^i{}_3)_4]$, is compositionally analogous to but structurally different from the $[Fe_8S_8]^0$ core of known clusters. The clusters are topological isomers. The cobalt cluster is a rhomb-bridged noncubane (RBNC), and the iron cluster is an edge-bridged double cubane (EBDC). Core relative stabilility may be related to valence electron count. A conceptual model for the RBNC ↔ EBDC interconversion is presented. The EBDC structure is populated by homometallic Fe_8S_8 and heterometallic $M_2Fe_6S_8$ clusters, whereas the RBNC structure is currently known only for Co_8Q_8 (Q = S, Se) clusters.

Acknowledgment. This research was supported at Harvard University by NIH Grant GM 28856.

Supporting Information Available: X-ray crystallographic files in CIF format for the seven compounds in Table S-1, bond angles and distances, selected interatomic distances and angles of **3**−**6**, magnetic data for compounds **1** and **2**, calculated spin manifold energies, and structural depictions of clusters **7** and **8**. This material is available free of charge via the Internet at http://pubs.acs.org.

JA903847A